UNIVERSITY
OF TRENTO

DIPARTIMENTO DI INGEGNERIA E SCIENZA DELL'INFORMAZIONE

38123 Povo – Trento (Italy), Via Sommarive 14
http://www.disi.unitn.it

MORPHOLOGICAL PROCESSING OF ELECTROMAGNETIC SCATTERING DATA FOR ENHANCING THE RECONSTRUCTION ACCURACY OF THE ITERATIVE MULTI-SCALING APPROACH

D. Franceschini, A. Rosani, M. Donelli, A. Massa, and M. Pastorino

January 2011

Technical Report # DISI-11-253

Morphological Processing of Electromagnetic Scattering Data for Enhancing the Reconstruction Accuracy of the Iterative Multi-Scaling Approach

Davide Franceschini[1], Andrea Rosani[1], Massimo Donelli[1],
Andrea Massa[1], and Matteo Pastorino[2]

[1]Department of Information and Communication Technology, University of Trento
Via Sommarive 14, I-38050 Trento, Italy
E-mail: *andrea.massa@ing.unitn.it*, Web-page: *www.eledia.ing.unitn.it*

[2]Department of Biophysical and Electronic Engineering, University of Genoa
Via Opera Pia 11A, 16145 Genova, Italy
E-mail: *pastorino@dibe.unige.it*

Abstract *– This work presents a methodology to locate and characterize multiple unknown scatterers exploiting the scattered electromagnetic radiation collected on a measurement region outside the area under investigation. In many practical cases, an accurate quantitative imaging of the scenario under test is required and it can be reached by using a high resolution representation of the dielectric profile of the scatterers. Towards this aim, an enhanced iterative multi-resolution procedure that exploits a morphological processing for detecting and focusing on different non-connected regions-of-interest has been developed.*
A suitable set of representative numerical results will demonstrate that the proposed approach is able to efficiently detect the objects in the imaging scenario and to enhance the accuracy in reconstructing multiple scatterers.

Keywords – Microwave Imaging, Inverse Scattering, Multiresolution, Morphological operations.

I. INTRODUCTION

Microwave imaging techniques are based on the processing of the scattered electromagnetic radiation collected on a measurement domain lying outside the region to be investigated. Such methodologies find a variety of applications in biomedical sciences (e.g., breast cancer imaging [1]), in the context of the subsurface inspection [2] and of the non-destructive industrial testing [3].

Whatever the application, the information content of the problem data turns out to be intrinsically bounded [4] and thus an accurate quantitative imaging of the scenario under test is unavoidably limited. Therefore, this issue needs particular attention since every practical application requires the representation of the dielectric or conductivity profiles with the highest achievable level of resolution.

In this context, different kinds of multiresolution approaches have been proposed [5]-[9] in order to meet the accuracy requirements even in presence of a limited amount of informative field measures. These techniques avoid a fine and homogeneous discretization in the whole investigation domain by properly employing a high resolution level only in some regions-of-interest (RoIs) inside the area under test.

Pursuing this idea, *Miller et al.* [5][6] proposed statistically-based approaches, while other works introduced a wavelet expansion [7][8] of the test domain. Successively, the Iterative Multi-Scaling Algorithm (IMSA) has been presented in [9]. Such a methodology is able to iteratively reconstruct an unknown scenario exploiting an adaptive allocation of the resolution levels according to the information gained during a multi-step retrieval process. Therefore, an enhanced resolution in the regions-of-interest is guaranteed, since the amount of information collected through the field measurement is efficiently exploited. Notwithstanding the effectiveness of the IMSA in many scenarios, it presented some limitations in dealing with multiple-scatterers configurations. Thus, the integration of a suitable procedure able to localize multiple objects in a search domain was mandatory. Certainly, many different approaches could be, in principle, integrated in the IMSA, as for example the method of decomposition of the time reversal operator (DORT) [10] or the level set method [11]. The former allows to locate a set of unknown scatterers by means of a very robust approach with low sensitivity to the noise, but the sizes of the scatterers have to be smaller than half a wavelength and the objects should be separated by more than a third of a wavelength. The second one is also very effective in determining the location and the shape of unknown obstacles but it requires the knowledge of the dielectric parameters of the scatterers under test. Moreover, a technique for finding the minimum circular envelope enclosing a set of scatterers and successively localize them has been proposed in [12]. Even though it avoids the solution of the full inverse problem, such an approach cannot provide any estimation of the extension of the RoIs.

As a matter of fact, in several applications a quantitative characterization of the dielectric properties of multiple RoIs is

required and the localization or the shaping of the scatterers is not enough. For this reason an improved version of the IMSA has been proposed in [13] by integrating a clustering procedure [13] between successive steps of the multi-scaling algorithm. The numerical and the experimental assessment have demonstrated the accuracy of the approach in resolving different non-connected regions-of-interest exploiting a suitable processing of intermediate reconstructions. The pixel representation of the retrieved profile is firstly binarized by thresholding the arising image according to the histogram analysis. Successively, a scanning of the image allows the detection and the definition of the RoIs in which the scatterers are located and where the resolution level can be increased. Unfortunately, such a procedure presents some deficiencies in dealing with complex scenarios and therefore a new set of morphological transformations [14][15] has been developed and integrated in the multi-scaling algorithm (let us call the new approach M-IMSA) in order to substitute the clustering procedure described in [13]. Such a new strategy allows a more detailed detection of the RoIs with a limited increase of the overall computational burden.

This paper will be structured as follows; in Sect. II the mathematical formulation of the morphological processing for the RoIs definition and its integration in the IMSA will be presented; in Sect. III a comparative analysis will be carried out in order to assess the advantages and the robustness of the proposed approach with respect to that described in [13]; in Sect. IV some conclusions will be drawn.

II. PROBLEM FORMULATION

The two-dimensional geometry of Fig. 1 representing a cross sectional view of an inhomogeneous investigation domain D_I will be considered in the following. Such a scenario is sensed illuminating it with a set of monochromatic incident electric fields TM polarized impinging from V different directions ($E_v^{inc}(x,y)\hat{\underline{z}}$, $v=1,...,V$).

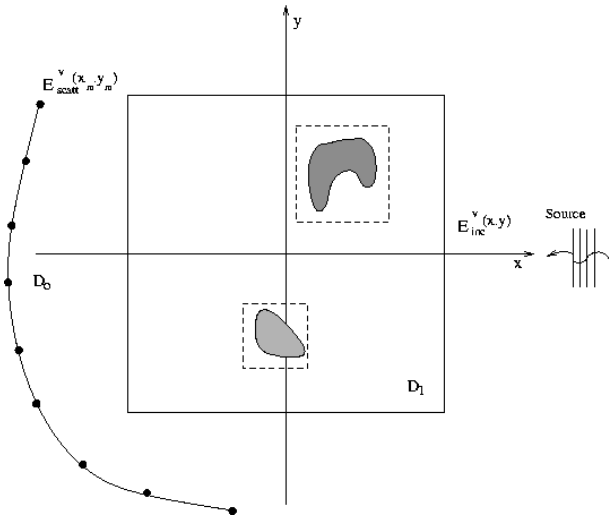

Fig. 1 Problem geometry

The properties of the structures under test are modeled through the object function $\tau(x,y)$ defined as follows

$$\tau(x,y)=\varepsilon_r-1-j\frac{\sigma(x,y)}{\omega\varepsilon_0} \qquad (1)$$

where ε_r and σ denote the relative permittivity and the conductivity, respectively.

The measures of the scattered field ($E_v^{scatt}(x_m,y_m)\hat{\underline{z}}$, $v=1,...,V$) are collected at $m=1,...,M$ positions belonging to the measurement domain D_O located outside D_I . These data are related to the contrast function $\tau(x,y)$ by means of the well known integral equations [16]

$$E_v^{scatt}(x_m,y_m)=S_v^{ext}\left[\tau(x_n,y_n),E_v^{tot}(x_n,y_n)\right] \qquad (2)$$

$$E_v^{inc}(x_n,y_n)=E_v^{tot}(x_n,y_n)-S_v^{\text{int}}\left[\tau(x_n,y_n),E_v^{tot}(x_n,y_n)\right] \qquad (3)$$

where $S_v^{ext}[\cdot]$ and $S_v^{\text{int}}[\cdot]$ indicate the external and internal scattering operators [16], respectively. $\tau(x_n,y_n)$ and $E_v^{tot}(x_n,y_n)$ ($n=1,...,N$) are the unknowns whose N-dimensional finite representation has to be reconstructed by solving a non linear problem characterized by intrinsic ill-posedness.

Moreover, an efficient allocation of the unknowns and thus of the discretization grid in the regions-of-interest (RoIs) of D_I is necessary because of the intrinsic bound in the amount of information collectable from the field measures.

To accomplish this, the M-IMSA approach aims at defining through a multi-step ($s=1,...,S_{opt}$) procedure a multiresolution distribution of the unknowns space according to the flow chart of Fig. 2, where the sequence of the main M-IMSA operations and the integrated morphological processing is reported. The structure of the algorithm can be subdivided in four macro blocks: a *profile retrieval* stage, a *profile processing* stage, a *convergence check* and a *resolution allocation* stage.

A. *Profile retrieval*

After the initialization stage, the number of RoIs is set to $I^{(0)}=1$ and $D_{RoI(0)}^{(1)}\equiv D_I$ because no a-priori information on the scenario under test is assumed. Successively, a multi-step cost function is defined as follows

$$\Phi^{(s)}=\Phi_{Data}^{(s)}+\Phi_{State}^{(s)} \qquad (4)$$

where

$$\Phi_{Data}^{(s)}=\frac{\sum_{v=1}^{V}\sum_{m=1}^{M}\left|E_v^{scatt}(x_m,y_m)-S_v^{ext}\left[\tau(x,y),E_v^{tot}(x,y)\right]\right|^2}{\sum_{v=1}^{V}\sum_{m=1}^{M}\left|E_v^{scatt}(x_m,y_m)\right|^2} \qquad (5)$$

$$\Phi_{State}^{(s)}=\frac{1}{\sum_{v=1}^{V}\sum_{m=1}^{N}\left|E_v^{inc}(x_n,y_n)\right|^2}\left\{\sum_{v=1}^{V}\sum_{n=1}^{N}\left|E_v^{inc}(x_n,y_n)-E_v^{tot}(x_n,y_n)+S_v^{\text{int}}\left[\tau(x_n,y_n),E_v^{tot}(x_n,y_n)\right]\right|^2\right\} \qquad (6)$$

in order to look for the optimal unknowns configuration that can be related to the problem data through the scattering model described by eq. (2) and (3).

When the problem is formulated in such terms, the functional (4) can be minimized with any available optimization tool (e.g., [17] - [19]) and the reconstructed image of the object function distribution can be processed to acquire information about the number of RoIs ($I^{(s)}$) in D_I and their extension $\left(D_{RoI(s)}^{(i)}\right)$.

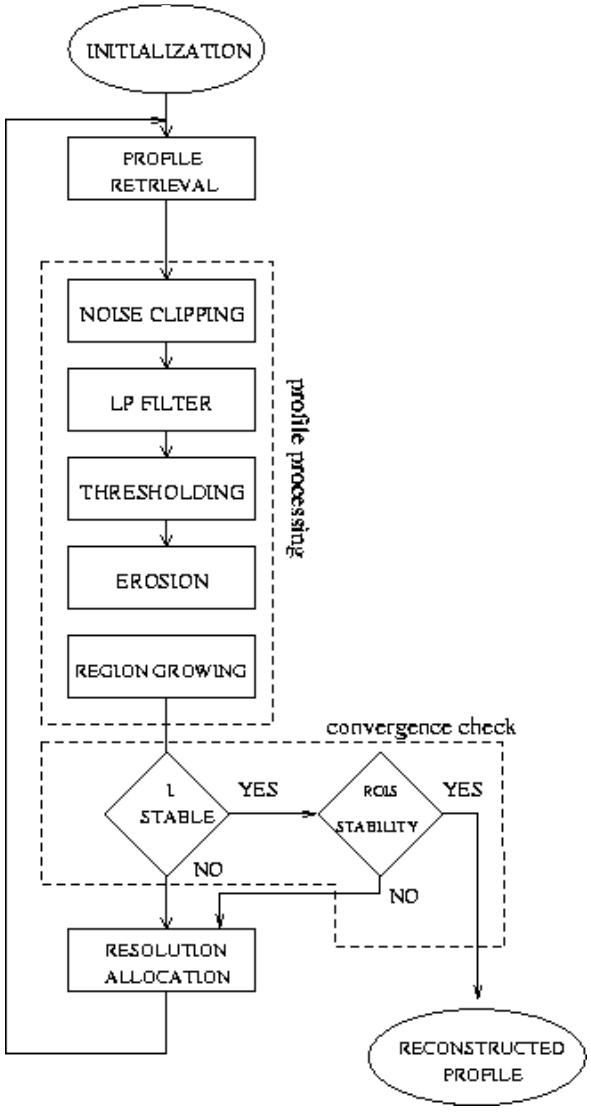

Fig. 2. The flow chart of the M-IMSA strategy.

B. *Profile processing*

Each image of the retrieved profiles can be processed with the set of morphological operations described in the following. Firstly, a *noise clipping* stage reduces the presence of the image noise thus avoiding an overestimate of the number of RoIs. Thanks to such an operation a new distribution of the object function is obtained as follows

$$\tau_{nc}^{(s)}(x_n, y_n) = \begin{cases} 0 & if\ \ \tau^{(s)}(x_n, y_n) \le \eta \\ \tau^{(s)}(x_n, y_n) & if\ \ \tau^{(s)}(x_n, y_n) > \eta \end{cases} \quad (7)$$

where $\eta = \mu \max\left\{\tau^{(s)}(x_n, y_n)\right\}$ and μ is a parameter which value has to be heuristically calibrated. In order to obtain a smother distribution and reduce the intensity of the artifacts, a Low Pass Filtering of the image of $\tau_{nc}^{(s)}$ is performed by applying the following weighted average over a neighborhood of the L=9 pixels centered around (x_n, y_n)

$$\tau_f^{(s)}(x_n, y_n) = \alpha\, \tau_{cl}^{(s)}(x_n, y_n) + \sum_{p=-1}^{1}\sum_{t=-1}^{1} \beta\, \tau_{cl}^{(s)}(x_{n+p}, y_{n+t}) \quad (8)$$

with $p + t \neq 0$.

The intensity of the filtering is determined by the parameters α and β

$$\alpha = 1 - \frac{\chi + 20}{100} \quad (9)$$

$$\beta = \frac{\chi + 20}{100} \frac{1}{(L-1)} \quad (10)$$

where χ is a parameter heuristically selected during the calibration of the thresholding stage. This latter operation is aimed at clearly defining the objects in the scenario under test by applying the following binary transformation to $\tau_f^{(s)}$

$$\tau_T^{(s)}(x_n, y_n) = \begin{cases} 0 & if\ \ \tau_f^{(s)}(x_n, y_n) \leq \kappa \\ 1 & if\ \ \tau_f^{(s)}(x_n, y_n) > \kappa \end{cases} \quad (11)$$

where $\kappa = \chi \max\left\{\tau_f^{(s)}(x_n, y_n)\right\}$.

After binirizing the image of the object function distribution, the *erosion* of the profiles shape provides an estimation of the number of RoIs ($I^{(s)}$) lying in the area under test. Towards this aim, a square *structuring element* Σ process the image $\tau_T^{(s)}$ considering a window of $L_\Sigma = 3 \times 3$ neighborhood pixels that defines another binary image according to the following rule

$$\tau_E^{(s)}(x_n, y_n) = \begin{cases} 1 & if\ \ \tau_T^{(s)}(x_n, y_n) = 1 \wedge \\ & \sum_{p=-1}^{1}\sum_{t=-1}^{1} \tau_T^{(s)}(x_{n+p}, y_{n+t}) = 1 \\ 0 & otherwise \end{cases} \quad (12)$$

in order to isolate at least one pixel (*seed*) per object.

Then, the region-of-interest to which a seed belongs to is determined by finding the minimum square area including the subset of non-zero pixels around the considered seed.

C. *Convergence check*

The macro block of the profile processing operations is able to estimate the number of RoIs, their position and their extension. By means of these informations it is possible to determine the convergence of the M-IMSA algorithm according to the criteria described in [13] related to the stability of the parameter $I^{(s)}$ and of the geometrical parameters of the RoIs.

D. *Resolution allocation*

If the convergence check does not hold true, the set of basis function is split in the $I^{(s)}$ regions as follows

$$N_i^{(s)} = INT\left[\left(N^{(1)} \frac{A_i^{(s)}}{\sum_{i=1}^{I^{(s)}} A_i^{(s)}}\right)^{\frac{1}{2}}\right] \quad (13)$$

in which $A_i^{(s)}$ is the area of the i-th region at the s-th step of the M-IMSA and the function $INT[\cdot]$ provides the greater integer of its argument.

As a matter of fact, the spatial resolution in the RoIs of D_I is increased and the accuracy of the profiles reconstruction can be further improved (see the flow chart in Fig. 2) performing another optimization of the cost function (4).

III. NUMERICAL ANALYSIS

In this Section a multiple object configuration will be considered in order to point out the effectiveness and the improvements allowed by the M-IMSA. As far as the imaging set up is concerned, an incident plane wave impinging from $V = 8$ different equally-spaced directions has been assumed and the field measures are collected at $M = 15$ positions on a circular observation domain of radius $2\lambda_0$. In order to blur the problem data, a Gaussian noise characterized by $SNR = 20dB$ has been added to the simulated scattered field values.

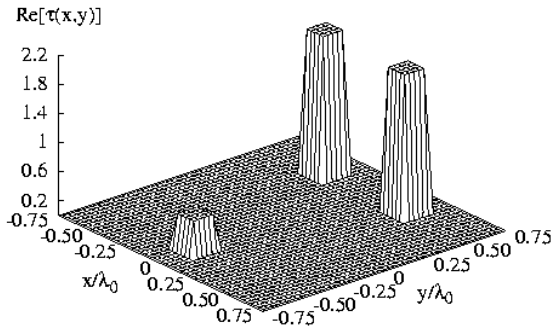

Fig. 3. Original distribution of the reference profile.

As a preliminary assessment, the configuration shown in Fig. 3 has been considered. It is characterized by three $0.15\lambda_0$-sided square homogeneous dielectric ($\tau_1 = \tau_2 = 2.0, \tau_3 = 0.5$) scatterers located in a square investigation area $L_{D_I} = 1.5\lambda_0$-sided. The three objects are located at ($x_o^{(1)} = -x_o^{(2)} = -0.3\lambda_0$, $y_o^{(1)} = y_o^{(2)} = 0.525\lambda_0$) and ($x_o^{(3)} = 0.0\lambda_0$, $y_o^{(3)} = -0.525\lambda_0$). The investigation domain has been initially partitioned in $N^{(1)} = 144$ square subdomains.

As far as the morphological processing is concerned, extensive simulations has suggested to set $\mu = 15$ in order to remove the image noise without significantly altering the object function distribution. Moreover, with a similar heuristic procedure, the value of $\chi = 25$ has been selected as a good trade-off between robustness (overestimation) and effectiveness (RoIs closer to the actual ones) of the regions-of-interest definition.

The distribution reconstructed at the first step (s=1) of the M-IMSA is shown in Fig. 4(*a*). The set of morphological operations described in Sect. II is applied to such a profile and the binary image of Fig. 4(*b*) points out the RoIs detected at the first step. Three different regions can be clearly defined by the erosion and region growing stages with a completely unsupervised methodology.

Successively, the resolution is increased in the RoIs according to eq. (13) and the cost function is again minimized. The result of the second (s=2) step of minimization is shown in Fig. 5(a). The accuracy of the estimated contrast is improved, as well as the effectiveness of the morphological operations in refining the extensions and the positions of the RoIs. Eventually, the last step of minimization provides the convergence profile ($s = S_{opt} = 3$) displayed in Fig. 5(*b*): the stronger scatterers are clearly improved although the weak contrast is slightly deteriorated.

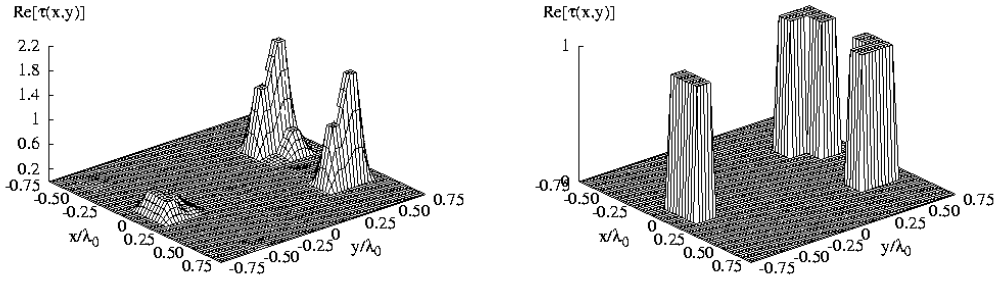

(*a*) (*b*)

Fig. 4. Homogeneous scatterers. (*a*) Reconstructed profile with SNR=20dB at the first step (s=1) of the M-IMSA and (*b*) result of the RoIs definition process.

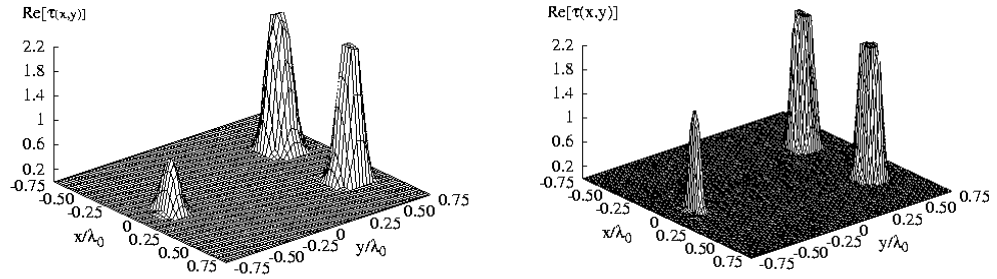

(*a*) (*b*)

Fig. 5. Homogeneous scatterers. Reconstructed profile by the M-IMSA with SNR=20dB when (*a*) s=2 and (*b*) s=3.

For comparison purposes, the reconstructed distribution obtained by means of the IMSA is shown in Fig. 6. It is immediately noticed how the retrieved distribution is not satisfactory, above all as far as the weak scatterer is concerned.

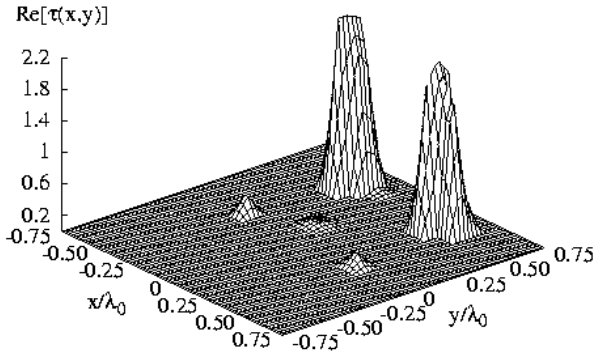

Fig. 6. Homogeneous scatterers. Reconstructed profile by the IMSA with SNR=20dB at the convergence step (*b*) s=3.

Such indications can be further confirmed by computing the overall reconstruction error, that for the M-IMSA approach is equal to 1.53% while is 2.41% for the standard implementation of the IMSA. The proposed approach overcome, then, the standard IMSA because the latter is not able to detect the RoI corresponding to the weak scatterer on the bottom of D_I, which is completely neglected during the optimization process from the second step onward.

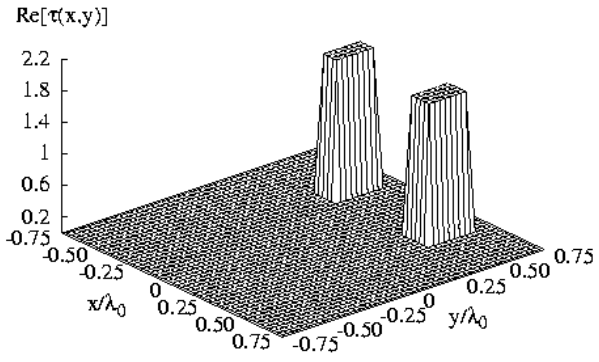

Fig. 7. Homogeneous scatterers. Image of the object function obtained by the IMSA at s=1 after thresholding.

Such a deficiency is due to the low robustness of the procedure detailed in [13]. In fact, in the considered test case, the reconstructed profile at s=1 is processed by thresholding with $T_\tau = 0.7$ [13] and the RoIs detected are shown in Fig. 7. The plot points out that the support of the third object is not revealed. On the contrary, the morphological processing integrated in the iterative multi-scaling approach allows to correctly detect the three RoIs and to retrieve the weak scatterer (Fig. 5) although it is located far from the stronger scatterers.

Eventually, the behavior of the $\Phi^{(s)}$ (Fig. 8) highlights the importance of an accurate estimation of the areas where the scatterers are located. In fact, the cost function of the IMSA suddenly increases at the second step when the support of the third object is lost and the minimization algorithm cannot retrieve a configuration of the unknowns that provides a good fitting in the considered cost functional.

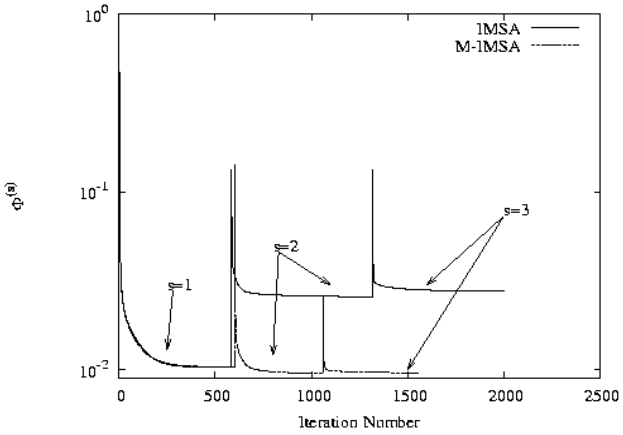

Fig. 8. Multiple homogeneous scatterers. Behaviour of the multi-step cost function minimization for the IMSA and the M-IMSA approaches.

IV. CONCLUSION

This paper has presented a selected set of numerical examples aimed at preliminarily assessing the iterative reconstruction of multiple scatterers integrated with a morphological processing stage. The proposed approach exploits a set of transformations in order to process the images of the intermediate reconstructions and estimated the position and the extension of the RoIs. By so doing, it is possible to increase the resolution level in such regions and considerable improve the accuracy of the retrieval process.

Accordingly, the numerical analysis concerned with a representative configuration of a multiple-scatterers scenario has shown as the M-IMSA is a more robust and accurate procedure for the identification of the RoIs with respect to the standard IMSA implementation. Certainly, further numerical and experimental test cases need to be considered in order to point out the effectiveness of the morphological transformations when the scatterers are in proximity of each others. Moreover, the class of the Coordinate Logic filters [20] will be object of study since they may also execute the morphological operators.

Finally, the presented procedure is expected be less efficient when there are variations in the background as in the case of subsurface imaging problems. This is a scenario of application that is currently under assessment.

ACKNOWLEDGMENT

The author wishes to thank Ing. L. Gasperotti for providing some of the numerical simulations.

REFERENCES

[1] J. M. Sill and E. C. Fear, "Tissue sensing adaptive radar for breast cancer detection - Experimental investigation of simple tumors models," *IEEE Trans. Microwave Theory Tech.*, vol. 53, pp. 3312-3319, Nov. 2005.

[2] Y. Yu, T. Yu, and L. Carin, “Three-dimensional inverse scattering of a dielectric target embedded in a lossy half-space,” *IEEE Trans. Geosci. Remote Sensing*, vol. 42, pp. 957-973, 2004.

[3] J. Ch. Bolomey, *Frontiers in Industrial Process Tomography*. Engineering Foundation, 1995.

[4] O. M. Bucci and G. Franceschetti, "On the degrees of freedom of scattered fields," *IEEE Trans. Antennas Propagat*., vol. 37, pp. 918-926, July 1989.

[5] E. L. Miller and A. S. Willsky, "A multiscale, statistically based inversion scheme for linearized inverse scattering problems," *IEEE Trans. Geosci. Remote Sensing*, vol. 34, pp. 346-357, Mar. 1996.

[6] E. L. Miller, "Statistically based methods for anomaly characterization in images from observations of scattered radiation," *IEEE Trans. Image Processing*, vol. 8, pp. 92-101, Jan. 1999.

[7] E. L. Miller and A. S. Willsky, "Wavelet-based methods for nonlinear inverse scattering problem using the extended Born approximation," *Radio Sci*., vol. 31, pp. 51-65, Jan. 1996.

[8] O. M. Bucci, L. Crocco, and T. Isernia, "An adaptive wavelet-based approach for non destructive evaluation applications," in *Proc. IEEE Antennas and Propagation Symp.*, vol. 3, pp. 1756-1759, 2000.

[9] S. Caorsi, M. Donelli, D. Franceschini, and A. Massa, "A new methodology based on an iterative multiscaling for microwave imaging," *IEEE Trans. Microwave Theory Tech.*, vol. 51, pp. 1162-1173, Apr. 2003.

[10] H. Tortel, G. Micolau, and M. Saillard, "Decomposition of the time reversal operator for electromagnetic scattering," *J. Electromagn. Waves Appl.*, vol. 13, pp. 687-719, Mar. 1999.

[11] A. Litman, D. Lesselier, and F. Santosa, "Reconstruction of two-dimensional binary obstacle by controlled evolution of a level-set ," *Inverse Problems*, vol. 14, pp. 685-706, June 1998

[12] O. M. Bucci, A. Capozzoli, and G. D'Elia, "A novel approach to scatterer localization problem," *IEEE Trans. Antennas Propagat*., vol. 51, pp. 2079-2090, Aug. 2003.

[13] S. Caorsi, M. Donelli, and A. Massa, "Detection, location, and imaging of multiple scatterers by means of the iterative multiscaling method," *IEEE Trans. Microwave Theory Tech.*, vol. 52, pp. 1217-1228, Apr. 2004.

[14] J. Serra, *Images Analysis and Mathematical Morphology*. New York: Academic Press, 1982.

[15] A. K. Jain, *Fundamentals of Digital Image Processing.* Englewood Cliffs, NJ: Prentice-Hall, 1989.

[16] D. Colton and R. Krees, *Inverse Acoustic and Electromagnetic Scattering Theory*, Berlin, Germany: Springer-Verlag, 1992.

[17] S. Y. Semenov, A. E. Bulyshev, A. Abubakar, V. G. Posukh, Y. E. Sizov, A. E. Souvorov, P. M. van den Berg, and T. C. Williams, "Microwave-tomographic imaging of the high dielectric-contrast objects using different image-reconstruction approaches," *IEEE Trans. Microwave Theory Tech.*, vol. 53, pp. 2284-2294, Jul. 2005.

[18] S. Caorsi, A. Massa, and M. Pastorino, "A computational technique based on a real-coded genetic algorithm for microwave imaging purposes," *IEEE Trans. Geosci. Remote Sensing*, vol. 38, pp. 1697-1708, Jul. 2000.

[19] M. Donelli and A. Massa, "Computational approach based on a particle swarm optimizer for microwave imaging of two-dimensional dielectric scatterers," *IEEE Trans. Microwave Theory Tech*., vol. 53, pp. 1761-1776, May 2005.

[20] B.G. Mertzios and K. Tsirikolias, "Coordinate Logic Filters and their Applications in Image Processing and Pattern Recognition," *Circuits, Systems and Signal Processing*, vol. 17, pp. 517-538, 1998.